ORIGINAL RESEARCH

Temperature-dependent and time-dependent effects of hyperthermia mediated by dextran-coated $La_{0.7}Sr_{0.3}MnO_3$: in vitro studies

Reihaneh Haghniaz
Rinku D Umrani
Kishore M Paknikar

Centre for Nanobioscience, Agharkar Research Institute, Pune, Maharashtra, India

Background: The purpose of this study was to investigate the therapeutic efficacy of dextran-coated (Dex) $La_{0.7}Sr_{0.3}MnO_3$ (LSMO) nanoparticles-mediated hyperthermia at different temperatures (43°C, 45°C, and 47°C) based on cell killing potential and induction of heat shock proteins in a murine melanoma cell (B16F1) line.

Methods: LSMO nanoparticles were synthesized by a citrate-gel method and coated with dextran. B16F1 cells were exposed to the Dex-LSMO nanoparticles and heated using a radiofrequency generator. After heating, the morphology and topology of the cells were investigated by optical microscopy and atomic force microscopy. At 0 hours and 24 hours post heating, cells were harvested and viability was analyzed by the Trypan blue dye exclusion method. Apoptosis and DNA fragmentation were assessed by terminal deoxynucleotidyl transferase-dUTP nick end labeling (TUNEL) assay and agarose gel electrophoresis, respectively. An enzyme-linked immunosorbent assay was used to quantify heat shock protein levels.

Results: Our data indicate that cell death and induction of heat shock proteins in melanoma cells increased in a time-dependent and temperature-dependent manner, particularly at temperatures higher than 43°C. The mode of cell death was found to be apoptotic, as evident by DNA fragmentation and TUNEL signal. A minimum temperature of 45°C was required to irreversibly alter cell morphology, significantly reduce cell viability, and result in 98% apoptosis. Repeated cycles of hyperthermia could induce higher levels of heat shock proteins (more favorable for antitumor activity) when compared with a single cycle.

Conclusion: Our findings indicate a potential use for Dex-LSMO-mediated hyperthermia in the treatment of melanoma and other types of cancer.

Keywords: hyperthermia, Dex-LSMO nanoparticles, heat shock proteins, melanoma, apoptosis

Introduction

"Hyperthermia" refers to a treatment procedure in which body temperature is increased to a few degrees above physiological temperature, between approximately 41°C and 47°C.[1] These high temperatures are reported to kill cancerous cells selectively and are thus useful in treating several types of cancer.[2–4] This effect is because of irregular and poor blood flow in the tumor that allows slow dissipation of heat, making cancerous cells more thermosensitive than normal cells.[5] Taking advantage of this differential thermotolerance, whole body hyperthermia is used clinically to treat cancer. However, a major concern with this type of treatment is the lack of local and uniform heating in the tumor region.[6] This is especially true for deep-seated tumors, where noninvasive external energy sources used for hyperthermia, such as warm water blankets, laser ablation, microwaves, and radiowaves, inevitably damage adjacent normal tissues.[6,7]

Correspondence: Kishore M Paknikar
Centre for Nanobioscience, Agharkar Research Institute, GG Agarkar Road, Pune 411 004, Maharashtra, India
Tel +91 20 2565 4831
Fax +91 20 2565 1542
Email kpaknikar@gmail.com

To overcome this problem, various strategies are being developed to achieve localized hyperthermia.

Radiofrequency (RF)-induced hyperthermia mediated by nanoparticles is a promising strategy for the treatment of cancer because RF energy can penetrate deeply into tissues. Using this method, nanoparticles that become excited on exposure to RF are deposited in the tumor to promote localized heating.[8,9] The improved heating efficiency because of the nanoparticles results in lowering of the RF field to a safe range (100–400 kHz), thereby minimizing nonspecific heating of healthy tissues.[10]

Among the different nanoparticles explored for hyperthermia, magnetic nanoparticles (MNPs) are of particular interest because of their many advantages. They can be targeted to tumor tissue using an external magnetic field[11] and removed once therapy is completed. Further, they can be used in combined biomedical applications, such as hyperthermia and magnetic resonance imaging.[12,13]

Application of MNPs in hyperthermia is based on their inherent property of heating upon exposure to an alternating magnetic field (eg, RF). The MNPs then dissipate the heat into the tumor tissue and selectively kill cancerous cells.[14] The mode of cell death depends on the temperature used for treatment, the duration of hyperthermia, and the vulnerability of the cells to heat.[15,16] Usually treatment at temperatures above 50°C (known as thermoablation) destroys tumor cells by necrosis, whereas treatment at a lower temperature (up to 47°C) results in apoptotic cell death.[17] Therefore, controlling the temperature during treatment is important. This highlights the need to either monitor the temperature during treatment or develop MNPs that stop heating once the required temperature is reached.[18]

Lanthanum strontium manganese oxide (LSMO; $La_{1-x}Sr_xMnO_3$) nanoparticles in a doping range of $0.2 \leq x \leq 0.3$ are of much interest owing to their low Curie temperature, which ranges from 320 to 370 K (47°C to 97°C), and their self-controlled heating properties.[19,20]

Based on this rationale, we examined the possibility of using LSMO nanoparticles as a hyperthermia agent in the treatment of cancer. LSMO nanoparticles were coated with dextran sulfate to improve their bioavailability and lessen their toxicity.[21] These dextran-coated (Dex)-LSMO nanoparticles were found to display a low Curie temperature (360 K) and self-controlled heating properties on exposure to RF.[22,23]

To evaluate the efficacy of hyperthermia mediated by Dex-LSMO nanoparticles, we selected murine melanoma (B16F1) cells as a cancer model, since this cancer is reported to be resistant to conventional treatment such as chemotherapy.[24]

Before treatment with hyperthermia, it was important to confirm that the Dex-LSMO nanoparticles themselves do not damage cells. We therefore evaluated the cytotoxicity of Dex-LSMO nanoparticles alone in various cell lines. As reported elsewhere,[21,23] we have noted a cell line-dependent and concentration-dependent cytotoxic effect of Dex-LSMO nanoparticles. Nevertheless, coating of LSMO with dextran could significantly reduce cytotoxicity as compared with bare LSMO.[21,23,25] Based on our previous research, a Dex-LSMO concentration of 250 µg/mL was found to be safe in melanoma cells and therefore was used in further experiments.[25]

The results of an internalization study was performed using fluorescence microscopy to investigate intracellular localization of nanoparticles.[25] Cells incubated with fluorescein isothiocyanate-conjugated Dex-LSMO nanoparticles showed rapid uptake of nanoparticles into the cytoplasm and nucleus. The observed internalization of Dex-LSMO nanoparticles could be important for delivery of therapeutic drugs directly into the intercellular compartment,[26] cell tracking, and contrast enhancement in magnetic resonance imaging.[25,27]

In our continued efforts, we evaluated induction of heat shock proteins (HSPs) in melanoma cells at different time points (ie, 0, 2, 4, 8, 12, 24, 48, and 72 hours) after treatment with hyperthermia at 43°C.[21] RF-induced Dex-LSMO-mediated hyperthermia resulted in enhanced induction of HSPs as compared with incubator hyperthermia (a model mimicking conventional whole body hyperthermia).[21] However, the mode of cell death and outcome of Dex-LSMO-mediated hyperthermia at temperatures higher than 43°C was not explored in those experiments. Thus, in the present work, we investigated the in vitro efficacy of Dex-LSMO-mediated hyperthermia at temperatures above 43°C (ie, 45°C and 47°C). The results are compared with hyperthermia at 43°C in terms of cellular morphology, mode of cell death, and induction of HSPs. We intend to use this information to select parameters for treatment of melanoma in our future in vivo studies.

Materials and methods
Materials
A murine melanoma (B16F1) cell line was obtained from the National Center for Cell Sciences, Pune, India. Dulbecco's Modified Eagle's Medium, fetal bovine serum, Hoechst 33342, and a Click-iT® terminal deoxynucleotidyl transferase-dUTP nick end labeling (TUNEL) Alexa Fluor® 594 Imaging Assay kit were obtained from Invitrogen

(Grand Island, NY, USA). Antibiotic–antimycotic solution (100×) and trypsin phosphate versene glucose were sourced from HiMedia Laboratories (Mumbai, India). Trypan blue, a GenElute Mammalian Genomic DNA Miniprep kit, radio-immunoprecipitation buffer, protease inhibitor cocktail, paraformaldehyde, standard heat shock proteins 70 and 90 (HSP70 and HSP90, respectively) and monoclonal antibodies (mAb70 and mAb90) were sourced from Sigma–Aldrich (St Louis, MO, USA). Triton™ X-100 and bovine serum albumin were purchased from Sisco Research Laboratories (Mumbai, India). Horse radish peroxidase-conjugated anti-antibody and tetramethylbenzidine (TMB)-H_2O_2 substrate were obtained from Bangalore Genei (Bangalore, India). A Lambda DNA/EcoRI + HindIII marker was purchased from Thermo Fisher Scientific (Waltham, MA, USA).

Synthesis and coating of nanoparticles

LSMO nanoparticles were synthesized by a citrate-gel method from metal acetate hydrate precursors as described elsewhere,[28] and were further coated using dextran sulfate sodium salt as explained in our earlier communication.[23] Briefly, presynthesized LSMO nanoparticles (200 mg) were dispersed in 10 mL of double-distilled water and bath-sonicated for 30 minutes. An equal concentration of dextran sulfate was added to the dispersion of LSMO nanoparticles and sonicated for another 30 minutes. The resulting mixture was shaken overnight at room temperature, ie, ~25°C, to obtain Dex-LSMO nanoparticles.

X-ray diffraction

Phase formation and the crystal structure of the LSMO sample were investigated using X-ray diffraction. Powder X-ray diffraction was performed with the help of a desktop X-ray diffractometer (Model MiniFlex II, Rigaku, Tokyo, Japan) with Cu Kα radiation (K value 0.9 and wavelength 1.5405 A°) and diffraction angle 2θ, ranging from 20° to 80°. The mean size of the crystallites was estimated using Scherrer's formula as shown below:

$$T = K\lambda/(B \cos\theta)$$

where T is the crystallite size, K is a constant, λ is the X-ray wavelength, B is the full width at half maximum of the diffracted peak, and θ is the angle of diffraction.

High-resolution transmission electron microscopy

High-resolution transmission electron microscopy (HRTEM) was carried out to determine the shape and particle size of Dex-LSMO. Samples were drop-coated on carbon-coated copper microgrids and allowed to air-dry. Images were then acquired using HRTEM (model Tecnai-T30, FEI Company, Hillsboro, NJ, USA) at an accelerating voltage of 300 kV.

Fourier transform infrared spectroscopy

LSMO and Dex-LSMO nanoparticles were analyzed by Fourier transform infrared spectroscopy (Model Spectrum One, Perkin Elmer Inc, Waltham, USA) to confirm dextran coating over the LSMO core. Dextran sulfate was used as a reference for comparison of characteristic peaks. Powder samples were mixed with potassium bromide and spectra were recorded in the 4,000–500 cm^{-1} wave number range.

Vibrating sample magnetometry

The magnetic moment of the nanoparticles was studied using a vibrating sample magnetometer (EG and G PAR 4500, Princeton Applied Research Corp, Princeton, NJ, USA). The magnetic moment was measured at room temperature (300 K), with an applied field (H) ranging from 0 to ±3,500 Oe.

RF-induced heating potential of Dex-LSMO nanoparticles

A high frequency generator (Model Hot Shot System 2, Ameritherm Inc, Scottsville, KY, USA) was used at a frequency of 365 KHz and a current of 700 A. The equipment consisted of a custom-made, water-cooled, five-turn spiral coil (Model ID 50 mm, Asetus Udyog, Bangalore, India) with an internal diameter of 50 mm. Various concentrations of nanoparticles (ie, 1, 5, and 10 mg/mL; total volume 1 mL) were prepared in phosphate-buffered saline (PBS), placed in the center of the coil, and exposed to RF. Increase in temperature was recorded up to 1,200 seconds using a fine spirit-filled thermometer. A plot of temperature versus time was drawn, and the specific absorption rate (SAR) value was calculated using the following formula:

$$SAR = \left(C_{solvent} / X_{magnetic\ element}\right) \times \left(dT/dt\right)$$

where $C_{solvent}$ is the specific heat capacity of water (4.18 J/gK), $X_{magnetic\ element}$ is the weight fraction of magnetic nanoparticles in the sample (g/L), and dT/dt is the initial slope of the temperature (K) versus time (seconds) curve. The time period of the first 150 seconds was considered for calculating the slope.

Optimization of hyperthermia

For optimization, unseeded tissue culture flasks containing Dex-LSMO nanoparticles (250 µg/mL in 5 mL culture medium) were used. Hyperthermia was applied using a pancake-shaped copper coil (Model ID 14 mm, Asetus Udyog) attached to an RF generator (Hot Shot System 2, Ameritherm Inc, Figure 1). Several parameters, ie, power of the instrument, frequency of RF, and period of exposure were tested, and the temperature rise was measured by placing a spirit-filled thermometer inside the flasks (as shown in the inset to Figure 1).

The B16F1 cells (5×10^5) were then seeded in 25 cm^2 tissue culture flasks containing 5 mL of Dulbecco's Modified Eagle's Medium (supplemented with 10% fetal bovine serum and 1% antibiotic–antimycotic solution) and allowed to grow for 48 hours at 37°C in the presence of 5% CO_2. Flasks not containing nanoparticles but exposed to RF served as the "RF" control. Culture flasks containing nanoparticles but not exposed to RF served as the "no RF" control.

Hyperthermia to B16F1 murine melanoma cells

After growing the B16F1 cells (5×10^5) in tissue culture flasks, a safe concentration of nanoparticles, ie, 250 µg/mL, was added to each flask to ensure that the Dex-LSMO nanoparticles per se do not cause cell death. The flasks were exposed to an optimized RF condition (365 kHz, input current 700 A, power 8,000 W) for a total time of 6, 8.5, and 11 minutes to increase the temperature from 37°C to 43°C, 45°C, and 47°C, respectively. After reaching the desired temperature, RF was switched off. To determine the effect of repeated cycles of hyperthermia, additional groups of cells were subjected to three cycles of hyperthermia at 15-minute intervals. All experiments were performed in triplicates.

Figure 1 Hot Shot System 2 radiofrequency generator attached to a pancake-shaped coil. The pancake-shaped coil used for the temperature rise in the cell culture flask is magnified in the inset.

Effect of hyperthermia on cell morphology

Cell morphology was viewed at 0 hours and 24 hours after treatment with RF-induced Dex-LSMO-mediated hyperthermia using an inverted optical microscope (Model TS 100, Nikon, Tokyo, Japan). Topological changes were imaged using an atomic force microscope (AFM, Model MultiView-1,000, Nanonics Imaging Ltd, Jerusalem, Israel). AFM images were processed using WSxM software (version 4.0, Nanotec Electronica, Madrid, Spain).

Effect of hyperthermia on cell viability

Cell viability was assessed by the Trypan blue dye exclusion method at 0 hours and 24 hours after RF-induced Dex-LSMO-mediated hyperthermia. After treatment, cells were collected by trypsinization, centrifuged, and the cell pellet was resuspended in 1 mL of PBS. Next, 10 µL of the resulting cell suspension was admixed with 10 µL of Trypan blue (0.4% in PBS). The numbers of nonstained (viable) cells and stained (dead) cells were counted using a hemocytometer. Cell viability was then calculated by the following formula:

$$\text{Viability}(\%) = \frac{\text{nonstained cells}}{\text{Stained cells} + \text{nonstained cells}} \times 100.$$

Three independent experiments were performed. The results were interpreted as the ratio of viable cells after hyperthermia treatment to that of the no RF control.

Detection of cell death by DNA laddering assay

Agarose gel electrophoresis was performed to assess the immediate (0 hours) and long-term (up to 48 hours) impact of RF-induced Dex-LSMO-mediated hyperthermia on induction of apoptosis. Cells were exposed to RF-induced hyperthermia. DNA was isolated from the heated cells at three different time points, ie, 0, 24, and 48 hours, using a GenElute Mammalian Genomic DNA Miniprep kit according to the manufacturer's instructions. Time points of 24 hours and 48 hours were included to allow DNA fragmentation to occur. Equal volumes of DNA samples (20 µL) were then loaded on 1% agarose gel (containing 5 µg/mL ethidium bromide in 1× Tris-acetate-ethylenediaminetetraacetic acid buffer, pH 8.5). Lambda DNA/EcoRI + HindIII was used as a marker and electrophoresis was carried out at 90 V for 1.5 hours. Fragments of DNA on the gel were then visualized under ultraviolet light.

Detection of cell death by TUNEL assay

To confirm the results of the DNA laddering assay and quantify the number of apoptotic cells, a TUNEL assay was performed using a Click-iT® TUNEL Alexa Fluor® 594 Imaging Assay kit.

For the experiment, 5×10^5 cells were grown on coverslips placed in Petri plates. After 48 hours, the cells were exposed to RF-induced Dex-LSMO-mediated hyperthermia (43°C, 45°C, or 47°C) . At 0 hours and after 24 hours of treatment, the cells were fixed with paraformaldehyde (4% solution in PBS) for 15 minutes and permeabilized with Triton X-100 (0.25% in PBS) for 20 minutes at room temperature. TUNEL staining followed, according to the manufacturer's protocol. Finally, the cells were counterstained with Hoechst 33342 for determination of the total cell number. Coverslips were mounted onto slides and observed using a fluorescence microscope (Model Eclipse E200, Nikon) under DAPI (excitation 330–380 nm, emission 435–485 nm for Hoechst) and tetramethylrhodamine (excitation 528–553 nm, emission 600–660 nm for TUNEL) filters. All images were captured at 400× magnification. The images were overlaid using Image-Pro plus software (version 6, Media Cybernetics Inc, Silver Spring, MD, USA) to confirm colocalization of the TUNEL signal with the nucleus.

To quantify the apoptotic cells, three independent cell counts (~100 cells per coverslip) were taken and the percentage of apoptotic cells was calculated using the following formula:

$$\text{Apoptotic cells}(\%) = \frac{\text{TUNEL apoptotic cells}}{\text{Total cells}} \times 100.$$

Effect of hyperthermia on HSP induction

Cells (5×10^5) were grown in 25 cm^2 culture flasks and exposed to hyperthermia. All the cells were then collected at 0 hours and 24 hours post treatment. Total protein was isolated using radioimmunoprecipitation buffer and protease inhibitor cocktail, according to the manufacturer's instructions.

Quantitative estimation of constitutive and inducible HSP70 and HSP90 was carried out by an indirect enzyme-linked immunosorbent assay method. Briefly, antigens (50 µL of isolated protein or HSP standards ranging from 2 to 15 µg/mL) were coated onto the surface of a 96-well microtiter plate at 4°C. On the following day, the wells were thoroughly washed with PBS. The remaining protein-binding sites in the coated wells were blocked by using blocking buffer (1% bovine serum albumin in PBS, 200 µL) and the plate was incubated at 4°C overnight. After thorough washing with PBS, 50 µL of monoclonal antibody at an optimized concentration (ie, 1:5,000 mAb70 or 1:2,000 mAb90 in blocking buffer) was added to the respective wells and the plate was incubated at room temperature for 2 hours. Wells were washed with PBS containing 0.05% Tween 20. Next, 50 µL of horseradish peroxidase-immunoglobulin G (1:5,000 in blocking buffer) was added to each well and incubated at room temperature for 2 hours. After thorough washing, 50 µL of substrate (TMB-H$_2$O$_2$) was added to each well and allowed to react in the dark for 30 minutes. Finally, the reaction was stopped by adding 12% H$_2$SO$_4$ (50 µL), and absorbance was read at 450 nm using a microplate reader (Model Synergy HT Multi-Mode, BioTek Instruments Inc, Winooski, VT, USA). The data were used to produce standard plots for HSP70 and HSP90. The concentrations of HSPs in the samples were then measured using standard plots and normalized to the cell numbers collected at the end of the treatment. The data are shown in picograms of HSP per cell.

Statistical analyses

The results are shown as the mean ± standard error of the mean of three replications. The statistical analysis was performed using one-way analysis of variance followed by Dunnett's multiple comparison test. A value of $P < 0.05$ was considered to be statistically significant.

Results and discussion
X-ray diffraction

The well-resolved peaks shown in Figure 2 could be indexed to the respective profiles of the interlattice plane distances d (hkl) of LSMO (JCPDS 47-0444), suggesting cubic symmetry of the crystal. No extra peaks were found, suggesting correct phase formation and phase purity of LSMO. The broad peaks in the X-ray diffraction spectrum pointed to a fine particle nature of LSMO. The size of the LSMO crystallite estimated by Scherrer's formula was ~20 nm.

High-resolution transmission electron microscopy

As reported earlier,[25] HRTEM images showed an irregular or nearly spherical shape of Dex-LSMO nanoparticles (Figure 3). A uniform layer of dextran around the LSMO core could be clearly observed (black arrows in Figure 3). The size of the Dex-LSMO nanoparticles was in a narrow range between 25 nm and 50 nm.
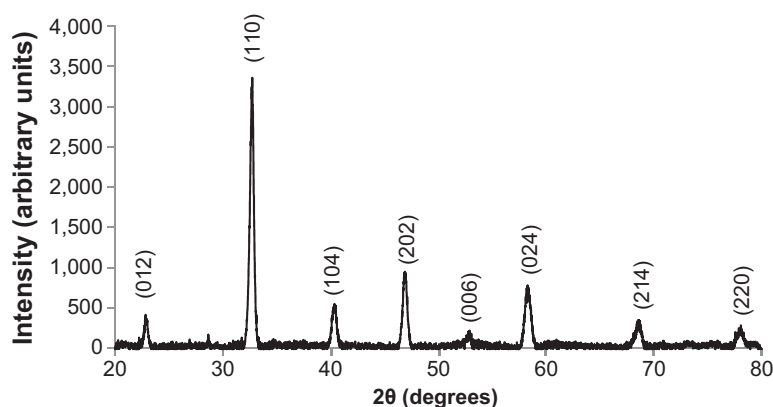
Figure 2 X-ray diffraction spectrum of LSMO nanoparticles.
Abbreviation: LSMO, $La_{0.7}Sr_{0.3}MnO_3$.

Fourier transform infrared spectroscopy

The Fourier transform infrared spectra obtained are shown in Figure 4. Both LSMO and Dex-LSMO spectra exhibited a characteristic band of Mn-O stretching (at 600 cm^{-1}) assigned to metal-oxygen bonds.[29] In the case of dextran sulfate, characteristic features at 1,100 cm^{-1} (C-O), 1,300 cm^{-1} (C-O), 1,650 cm^{-1} (C-O), 2,085 cm^{-1} (C-CH), 2,500 cm^{-1} (O-H), 2,950 cm^{-1} (C-H), and 3,500 cm^{-1} (O-H) could be seen. The strong O-H band at 3,500 cm^{-1} in the dextran sulfate spectrum weakened in the Dex-LSMO spectrum. That suggests possible electrostatic interaction of LSMO with dextran via O-H groups. In comparison with bare LSMO, additional peaks at 1,300 cm^{-1} and 1,650 cm^{-1} (C-O) in Dex-LSMO suggested dextran coating.

Vibrating sample magnetometry

It can be seen from the M-H curve (Figure 5) that the magnetic moment of the synthesized nanoparticles saturated at ~3,000 Oe. The saturation moment was found to be ~27 emu/g for bare LSMO and ~21 emu/g for Dex-LSMO nanoparticles. The lower saturation moment of Dex-LSMO could be attributed to their smaller size and the influence of coating on magnetization of the nanoparticles. Such magnetization drops have been reported after coating of LSMO with octadecylamine[30] or coating of iron oxide nanoparticles with silica.[31] Hysteresis loops (inset to Figure 5) revealed that LSMO and Dex-LSMO were predominantly ferromagnetic at room temperature. Importantly, the coercivity was found to be very small (less than 100 Oe), which could be due to the very small size of the particles.

RF-induced heating potential of Dex-LSMO nanoparticles

As can be seen in Figure 6, a concentration-dependent increase in temperature was observed upon exposure to RF, which was more pronounced within the first 300 seconds. The temperature of the Dex-LSMO nanoparticles at concentrations of 5 and 10 mg/mL rose to ~46°C within 300 seconds and 150 seconds, respectively, and then remained constant up to 1,200 seconds, suggesting "self-controlled" heating properties.

The estimated SAR value for Dex-LSMO at a concentration of 5 mg/mL was 23 W/g. The obtained SAR value is comparable with that reported for LSMO nanoparticles in the literature.[29,32]
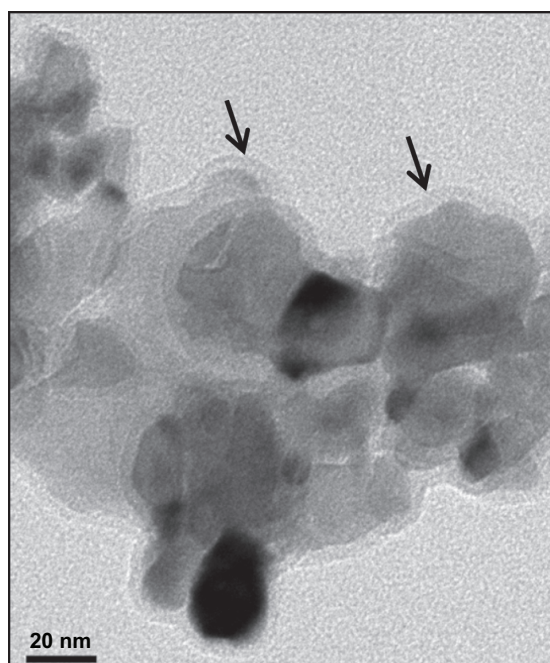
Figure 3 High-resolution transmission electron microscopy image of dextran-coated LSMO nanoparticles.
Notes: A uniform layer of dextran around the LSMO core can be observed (black arrows).
Abbreviation: LSMO, $La_{0.7}Sr_{0.3}MnO_3$.
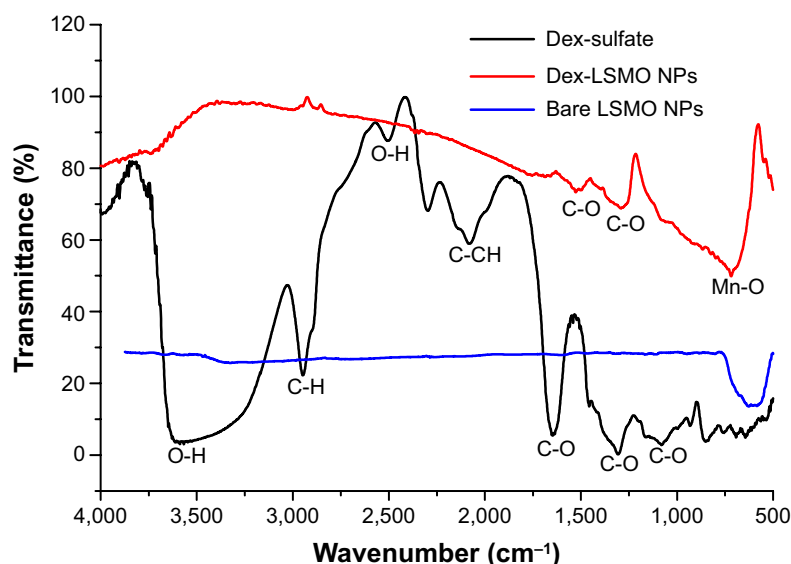
Figure 4 Fourier transform infrared spectra for Dex-sulfate, bare LSMO, and Dex-LSMO nanoparticles.
**Abbreviations:** Dex-sulfate, dextran sulfate sodium salt; Dex-LSMO, dextran-coated LSMO; LSMO, $La_{0.7}Sr_{0.3}MnO_3$; NP, nanoparticle.

Optimization of hyperthermia

As can be seen from Figure 7, cell morphology was unaltered in the no RF controls (flasks containing nanoparticles, but not exposed to RF) and RF controls (flasks free of nanoparticles but exposed to RF), indicating no effect of nanoparticles or RF treatment alone. Moreover, no significant temperature rise was observed in RF controls, indicating that RF per se could not result in heating; therefore, the temperature rise observed after exposure to RF is mediated by Dex-LSMO nanoparticles.

Effect of hyperthermia on cell morphology

It could be clearly seen by optical microscopy (Figure 8A) that cells exposed to RF-induced Dex-LSMO-mediated hyperthermia showed immediate (0 hours) morphological changes, ie, loss of cell extensions, rounding up and detachment at all temperatures, as compared with no RF controls. The cells heated up to 43°C regained their normal morphology after 24 hours of incubation in fresh growth medium; however, cells heated to 45°C and 47°C were not
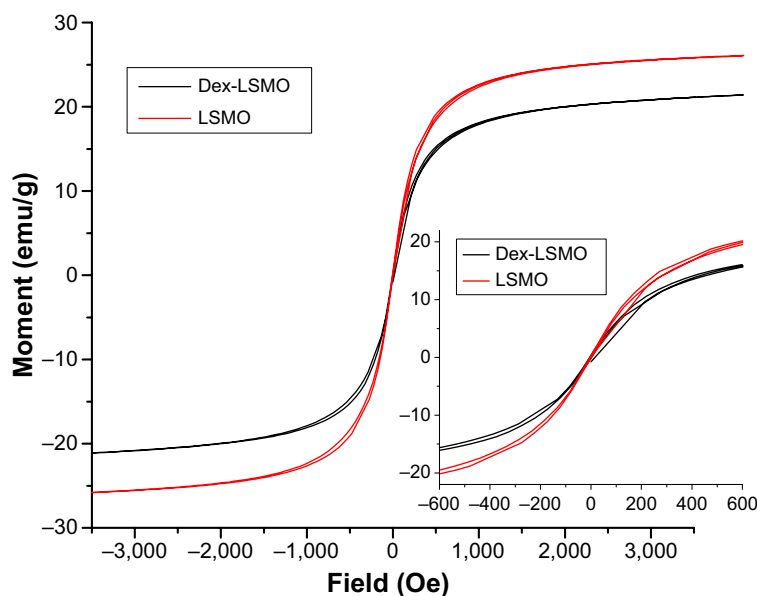
Figure 5 Plot of magnetic moment (M) versus field (H) at 300 K. Inset shows hysteresis loop for nanoparticles on an expanded scale.
Abbreviations: Dex-LSMO, dextran-coated LSMO; LSMO, $La_{0.7}Sr_{0.3}MnO_3$.
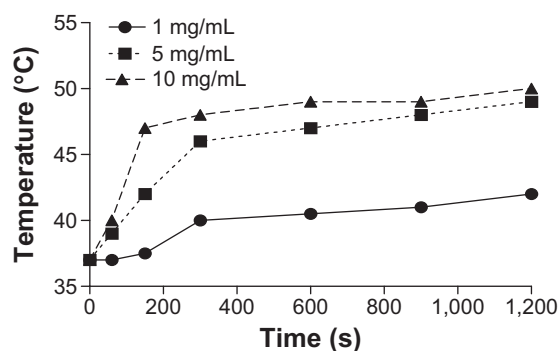
Figure 6 Induction heating curve for different concentrations of dextran-coated LSMO nanoparticles.
Abbreviation: LSMO, La$_{0.7}$Sr$_{0.3}$MnO$_3$.

able to revert to their normal slender morphology even after 24 hours of incubation.

Consistent with the optical microscopy results, AFM images of no RF control cells clearly showed defined boundaries with slender extensions joining neighboring cells (Figure 8B). After RF-induced Dex-LSMO-mediated hyperthermia at 43°C, 45°C, and 47°C, unclear boundaries and marked alterations in cell surface topology were observed at 0 hours (Figure 8B, upper panel). At 24 hours after treatment (Figure 8B, lower panel), cells that were heated at 43°C reverted to a stellate morphology with distinguishable boundaries and a clear nucleus, whereas the cells treated at 45°C and 47°C showed a markedly altered morphology.

To the best of our knowledge, this is the first report showing topological changes in cells after hyperthermia treatment, as seen by AFM. Nonetheless, several research groups have studied morphological changes in cells by optical microscopy after hyperthermia treatment at different temperatures (41°C–46°C) and heating periods.[16,21,33] We also observed temperature-dependent changes in cell morphology, as reported by other researchers. However, it must be pointed out that these studies mainly focused on the immediate response (at 0 hours) of cells after heat shock and ignored post treatment recovery.[34–36] In our experiment, cells were visualized not only at 0 hours (immediate changes) but also at 24 hours post treatment to assess the long-term behavior of the cells.

Garcia et al[37] observed immediate morphological changes in B16F10 cells after hyperthermia at 45°C, which increased in severity at 24 hours post treatment. These altered cells showed features of late apoptosis and necrosis on flow cytometry. Follow-up 14 days after hyperthermia demonstrated that the cells could not recover from the initial loss of viability occurring within 24 hours, indicating that the morphology at 24 hours post treatment determines the long-term fate of the cell. Thus, in case of Dex-LSMO hyperthermia at 45°C and 47°C, cell death is expected to be the final fate since the altered cell morphology did not revert to normal within 24 hours after treatment.

Effect of hyperthermia on cell viability

It has been reported that MNP-mediated hyperthermia can contribute to cell death by damaging the cell membrane.[9] Assuming that the effect of Dex-LSMO-mediated hyperthermia is the same, the Trypan blue assay, which is sensitive to membrane permeability, was performed to confirm the morphological changes observed after hyperthermia.

As can be seen in Figure 9, the viability of B16F1 cells was almost 100% in no RF controls, indicating that Dex-LSMO per se was not cytotoxic. A significant decline in cell viability (~15%) was seen immediately (0 hours) after a single cycle of hyperthermia at 43°C; although it remained constant up to 24 hours. On the other hand, cells treated at 45°C and 47°C showed a greater decrease in viable cell count at 0 hours after a single cycle of hyperthermia. As expected, hyperthermia at 47°C had a greater effect on cell viability as compared with 45°C. A resting period of 24 hours after a single cycle of
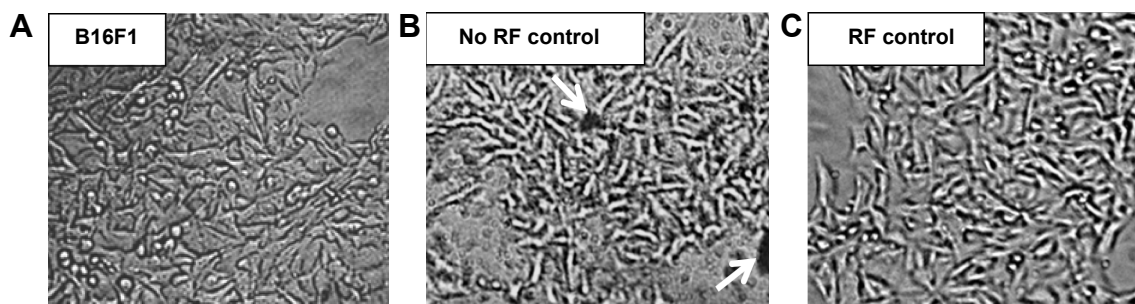
Figure 7 Optical microscopic images (100×) of (**A**) B16F1 cells, (**B**) no RF control cells, and (**C**) RF control cells. Arrows show aggregated dextran-coated LSMO nanoparticles.
Abbreviations: LSMO, La$_{0.7}$Sr$_{0.3}$MnO$_3$; RF, radiofrequency.

A

B
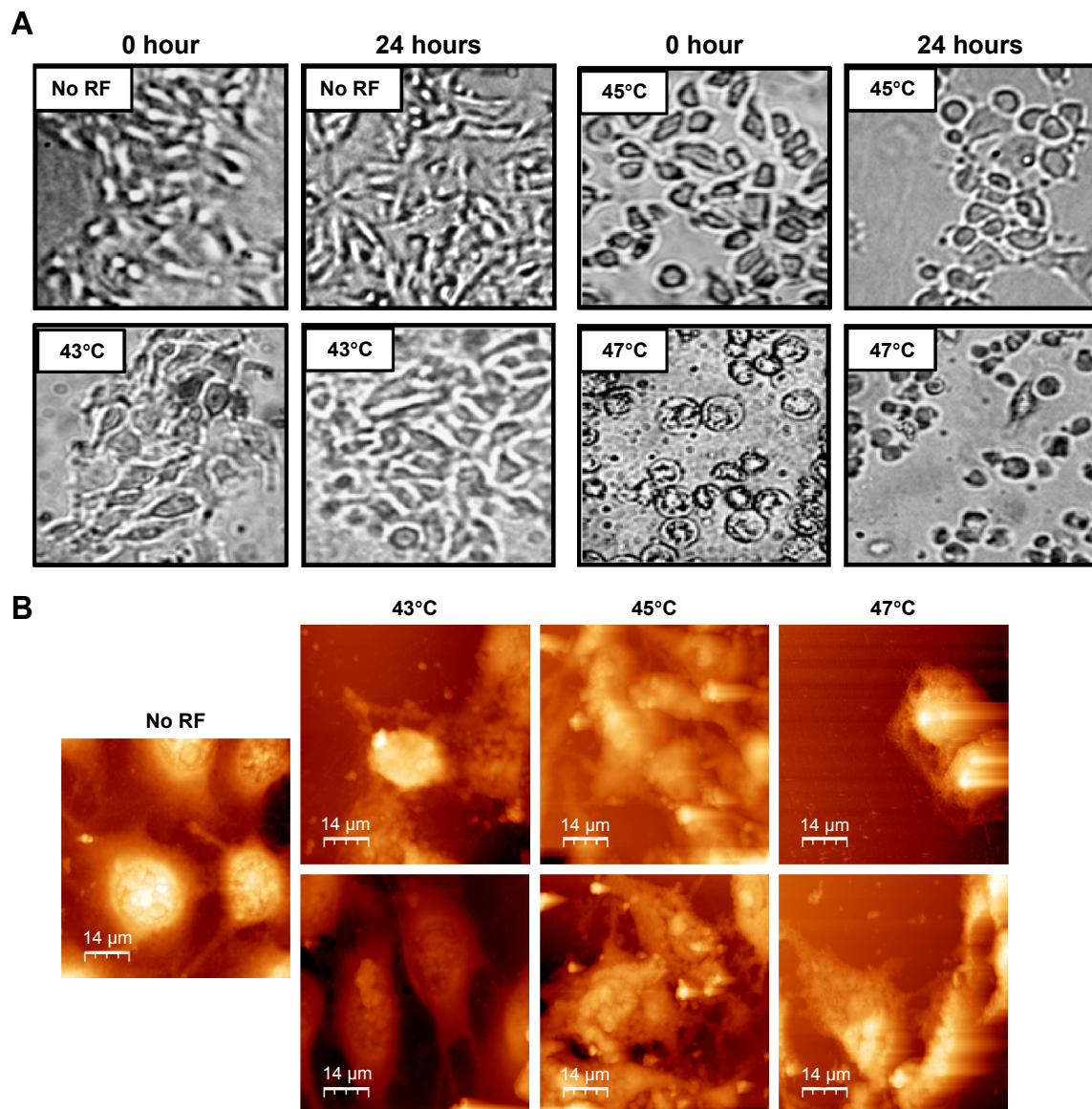
Figure 8 (**A**) Optical microscopic images (100×) of B16F1 cells at 0 hours and 24 hours after a single cycle of RF-induced dextran-coated LSMO-mediated hyperthermia at different temperatures. (**B**) Atomic force microscopy images of B16F1 cells, 0 hours (upper panel) and 24 hours (lower panel) after a single cycle of RF-induced dextran-coated LSMO-mediated hyperthermia at different temperatures as compared with no RF controls.
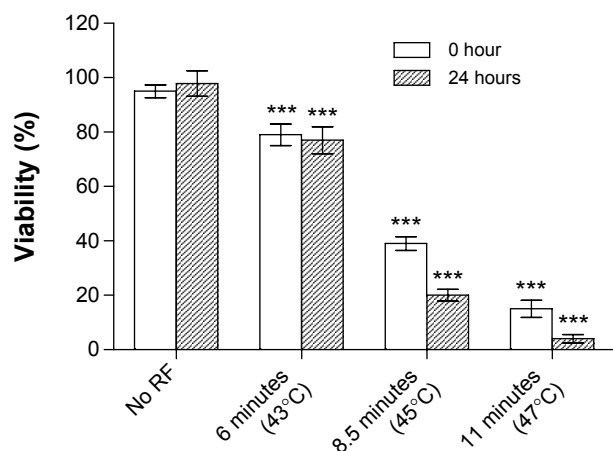
Abbreviations: LSMO, $La_{0.7}Sr_{0.3}MnO_3$; RF, radiofrequency.

hyperthermia further reduced the proportion of viable cells to 17% at 45°C and to 4% at 47°C.

Further, exposure of cells to repeated cycles of hyperthermia significantly reduced cell viability at 0 hours after treatment at all three temperatures (graph not shown). At 43°C, repeated hyperthermia could not further reduce cell viability after 24 hours, suggesting that cells can recover from heat shock at 43°C. Nevertheless, cells treated by repeated hyperthermia at 45°C and 47°C showed an ~100% reduction in viability after 24 hours of rest, suggesting that repeated cycles of hyperthermia is a more effective treatment as compared with a single cycle of hyperthermia.

Overall, our results suggest that Dex-LSMO-mediated hyperthermia reduces cell viability in a time-dependent and temperature-dependent manner and that a minimum temperature above 43°C is required to induce irreversible and significant cell death in melanoma cells.

In our previous study, melanoma (A375) cells showed a reduction in viability immediately after Dex-LSMO-mediated hyperthermia (43°C), but resumed proliferation within 72 hours.[21] Such a time-dependent and temperature-dependent decrease in cell viability has also been reported by other researchers; however, the extent of cell death varied depending on cell type, with some cells being more

Figure 9 Viability of B16F1 cells at 0 hours and 24 hours after a single cycle of RF-induced dextran-coated LSMO-mediated hyperthermia. ***$P<0.001$, one-way analysis of variance followed by Dunnett's test.
Abbreviations: LSMO, La$_{0.7}$Sr$_{0.3}$MnO$_3$; RF, radiofrequency.

susceptible to heat than others. For example, Ito et al[38] observed an instant cytostatic effect in rat T9 glioma cells after hyperthermia at 43°C, which continued for 24 hours, but then resumed to normal proliferation within 72 hours. Gao et al[39] reported excellent therapeutic efficacy of magnetite-mediated hyperthermia in KB cells, reducing cell viability by 56% and 78% at 45°C and 47°C, respectively.

## Detection of cell death by DNA laddering assay

During apoptosis, endogenous endonucleases cleave genomic DNA into oligonucleosome-sized fragments that are multiples of ~180–200 base pairs. When resolved on agarose gel, these fragments have a ladder appearance, which is accepted as a universal hallmark of apoptosis.[40,41] Thus, it was important to study whether Dex-LSMO-mediated hyperthermia induces DNA laddering in melanoma cells.

The electrophoretic pattern of DNA isolated from B16F1 cells treated with a single cycle of RF-induced Dex-LSMO-mediated hyperthermia is shown in Figure 10. It can be seen that at 43°C DNA remained intact, in a manner similar to that of the no RF controls, whereas DNA fragmentation appeared 48 hours after hyperthermia at temperatures of 45°C and 47°C.

This result suggests that heating at 43°C may not be able to induce apoptosis, and therefore, not suitable for the treatment of melanoma. However, there is a possibility of a false result because of the smaller population of apoptotic cells. It has already been reported that the DNA ladder may not be visible on agarose gel in biological systems with fewer apoptotic cells or with asynchronous apoptotic cells.[41] Therefore; it is likely that Dex-LSMO-mediated hyperthermia at 43°C induced apoptosis in a few cells but was not detectable in the laddering assay. Thus, the result needs to be confirmed by other methods, such as the TUNEL assay.

On the other hand, degradation of DNA by endonucleases is a late event in apoptosis as it requires activation of biochemical events involved in cleavage of DNA.[41] This might be the reason why DNA laddering was observed only at 48 hours following treatment at 45°C and 47°C in our experiments.
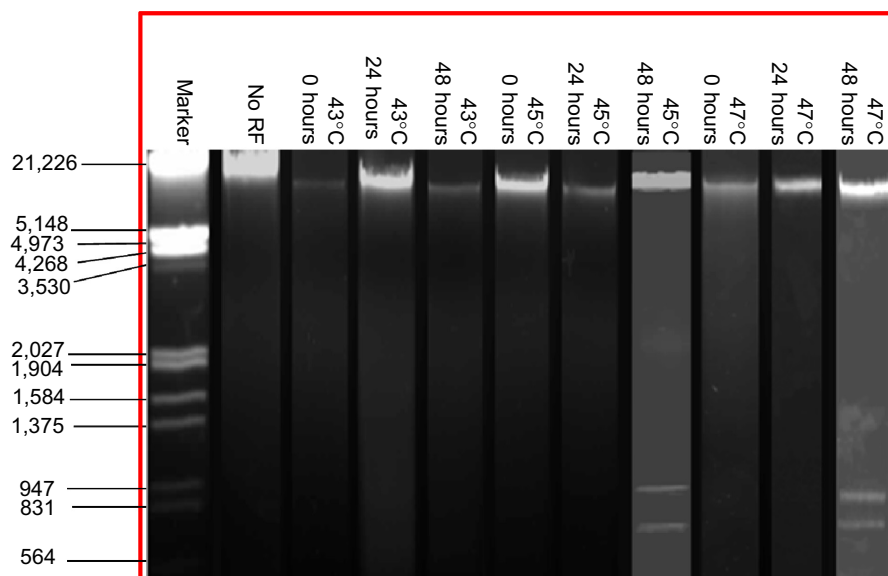
Figure 10 Gel electrophoresis of DNA extracted from B16F1 cells at different time points (ie, 0, 24, and 48 hours) after a single cycle of RF-induced dextran-coated LSMO-mediated hyperthermia.
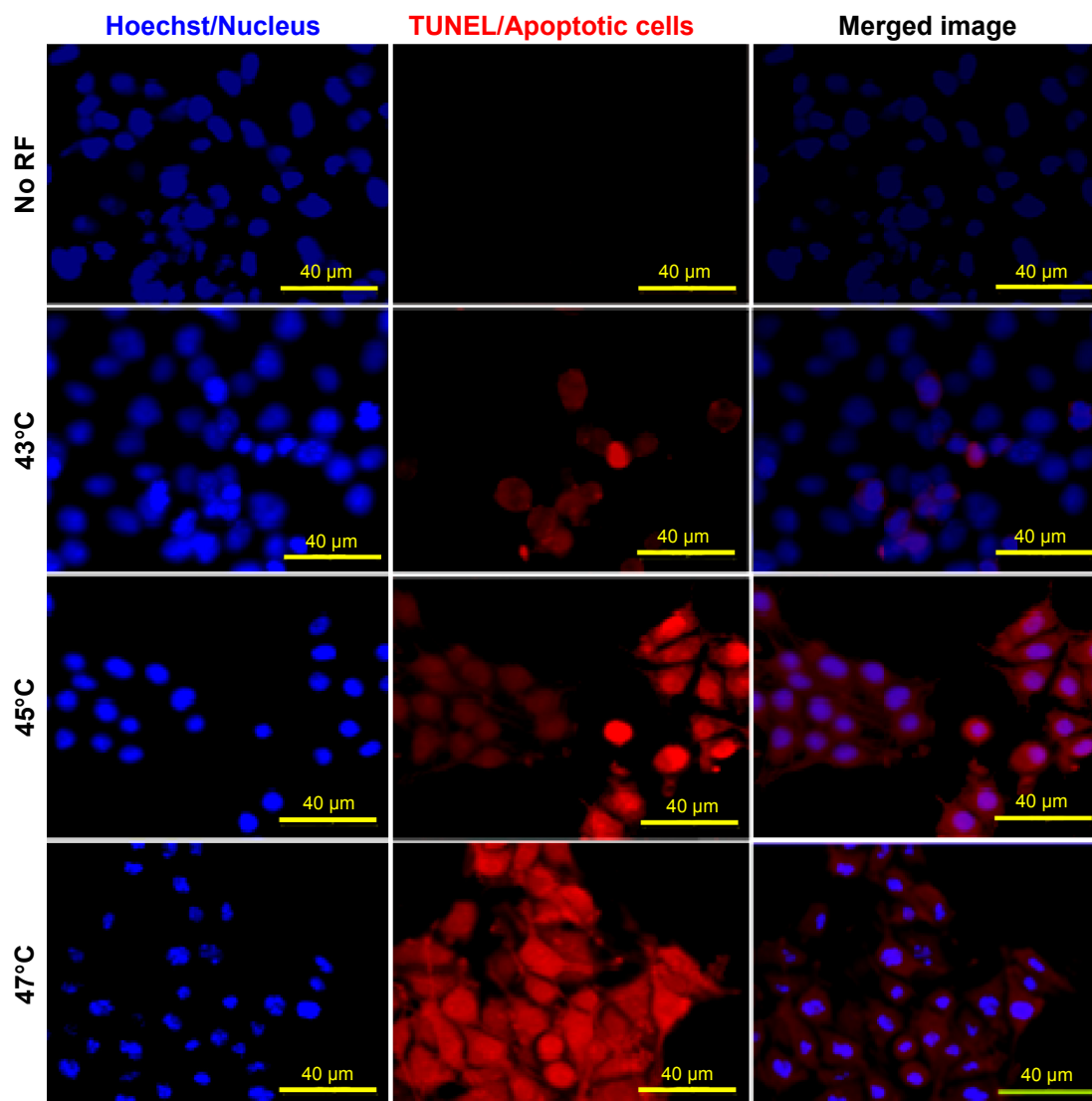**Abbreviations:** LSMO, La$_{0.7}$Sr$_{0.3}$MnO$_3$; RF, radiofrequency.

Unfortunately, we could not get results for three cycles of RF-induced hyperthermia in this experiment, because the majority of the cells detached from the flasks within 24 hours (probably due to rapid cell death) and a sufficient quantity of DNA could not be obtained.

Cell death detection by TUNEL assay

In contrast with DNA laddering assay, TUNEL staining can quantify apoptotic cells and detect DNA strand breakage in an individual cell.[41] We performed the TUNEL assay on our samples at 0 hours and 24 hours after hyperthermia. Representative fluorescence microscopic images of cells 24 hours after a single cycle of RF-induced hyperthermia at different temperatures are shown in Figure 11. Detection of

a TUNEL signal (apoptotic nuclei-specific red fluorescence) confirmed that apoptotic cell death occurred after hyperthermia at all the temperatures tested.

In the control sample (no RF), cells showed normal blue nuclei stained by Hoechst. At 43°C, a few apoptotic cells (red color) could be seen, while the majority of the cells were normal. At 45°C and 47°C, marked apoptosis was observed, as detected by an intense red color in the majority of cells. The TUNEL signal was colocalized with nuclei (merge images), confirming that the signal was due to DNA breakage and not background staining. Moreover, typical features of apoptotic cell death, namely condensed or fragmented nuclei, was clearly seen at 45°C and 47°C, which confirmed that DNA breakage was due to apoptosis not necrosis.

Figure 11 Hoechst/TUNEL staining of B16F1 cells 24 hours after a single cycle of RF-induced dextran-coated LSMO-mediated hyperthermia as compared with no RF control.
Abbreviations: LSMO, $La_{0.7}Sr_{0.3}MnO_3$; RF, radiofrequency; TUNEL, terminal deoxynucleotidyl transferase-dUTP nick end labeling.
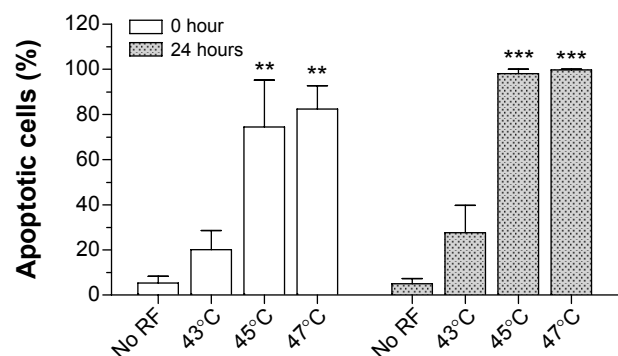
Figure 12 Percentage of apoptotic cells at 0 hours and 24 hours after treatment with a single cycle of RF-induced dextran-coated LSMO-mediated hyperthermia. **P<0.01, ***P<0.001, one-way analysis of variance followed by Dunnett's test.
**Abbreviations:** LSMO, $La_{0.7}Sr_{0.3}MnO_3$; RF, radiofrequency.

As mentioned earlier, hyperthermia treatment can induce either apoptotic or necrotic cell death, depending on the temperature applied. However, in terms of anticancer activity, apoptosis is recognized as an important mode of cell death, since it leads to genetically determined omission of a single cell, whereas necrosis is traumatic cell death in an unregulated fashion and mostly involves large numbers of cells. While necrosis eventually involves swelling of nuclei, apoptosis exhibits typical nuclear characteristics such as chromatin condensation and DNA fragmentation[42,43] which could also be seen in our study. The percentages of apoptotic cells determined by counting ~300 cells are shown in Figure 12. The apoptosis percentage at 0 hours after hyperthermia were ~20%, ~74%, and ~82% at 43°C, 45°C, and 47°C, respectively, whereas ≥98% of cells were found to be apoptotic 24 hours after treatment at temperatures of 45°C and 47°C.

When compared with no RF controls, apoptosis at 43°C was not statistically significant at both time points after treatment.

On the basis of the TUNEL results, a minimum temperature above 43°C is required for effective apoptosis in melanoma cells. The marked apoptosis and DNA fragmentation observed at 47°C suggests that a temperature of ~45°C might be needed to achieve maximum cell death by apoptosis and avoid unwanted necrosis. However, investigation of other markers involved in apoptosis, such as caspases, is necessary.

Effect of hyperthermia on induction of HSPs

The results of enzyme-linked immunosorbent assays for HSP70 and HSP90 are shown in Figure 13A and B, respectively. There were no changes in HSP levels in the no RF controls when compared with the B16F1 cells, indicating that Dex-LSMO nanoparticles per se could not induce production of HSPs whereas Dex-LSMO-mediated hyperthermia resulted in temperature-dependent induction of HSPs when compared with no RF controls. The HSP70 concentration increased by ~3-fold, ~4-fold, and ~13-fold at 0 hours and by ~9-fold, ~10-fold, and ~38-fold at 24 hours at 43°C, 45°C, and 47°C, respectively (Figure 13A). Likewise, the HSP90 concentration obtained was ~3-fold, ~5-fold, and ~13-fold at 0 hours, and ~2-fold, ~8-fold, and ~40-fold at 24 hours at 43°C, 45°C, and 47°C, respectively (Figure 13B). Taken together, these results show that induction of HSPs by hyperthermia increased with increasing temperature, and was higher at 24 hours post treatment when compared with 0 hours.
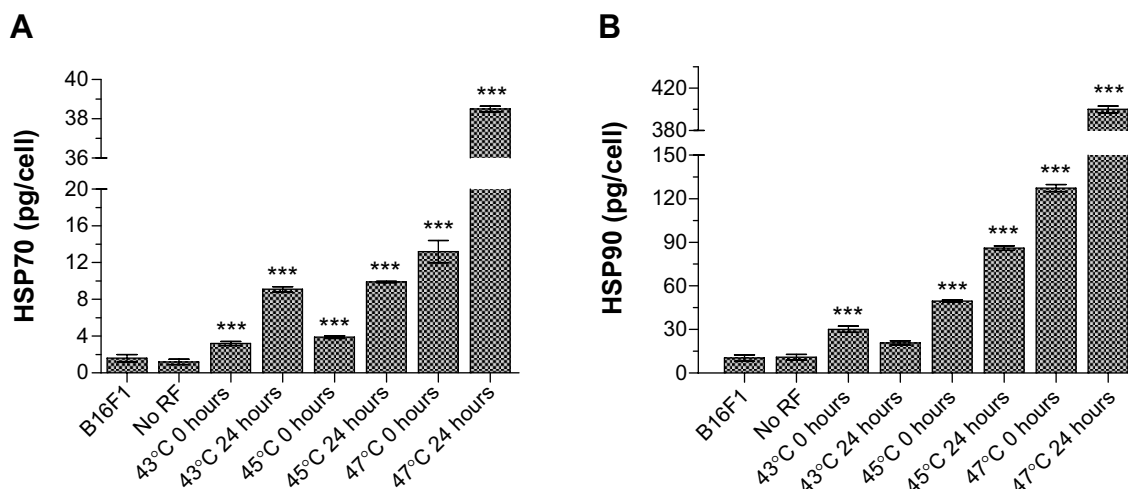
Figure 13 (**A**) HSP70 and (**B**) HSP90 induction at 0 hours and 24 hours after a single cycle of RF-induced dextran-coated LSMO-mediated hyperthermia. ***P<0.001, one-way analysis of variance followed by Dunnett's test.
Abbreviations: HSP, heat shock protein; LSMO, $La_{0.7}Sr_{0.3}MnO_3$; RF, radiofrequency.

Further, repeated cycles of hyperthermia were found to induce HSP levels that were higher than after a single cycle of treatment. Three cycles of RF-induced Dex-LSMO-mediated hyperthermia could increase the HSP70 level by ~10-fold, ~20-fold, and ~39-fold after heating at 43°C, 45°C, and 47°C, respectively (Figure 14A). However, the HSP90 level was not significantly increased after repeated cycles of RF-induced Dex-LSMO-mediated hyperthermia when compared with a single cycle (Figure 14B). The exact reason for the unaltered level of HSP90 after repeated cycles of hyperthermia has yet to be identified. However, it is suspected that the machinery involved in induction of HSP90 is more sensitive to heat than that for HSP70.

Studies carried out by other research groups using hematopoietic and erythroleukemia cells showed that hyperthermia at 42.5°C and 43°C could induce HSP70 soon after treatment,[44,45] which is in agreement with our observations. Vigor observed temperature-dependent effects (ranging from 38°C to 47°C) on induction of HSP70 after 30 minutes of incubator hyperthermia.[46] Ito et al[38] reported an increase in HSP70 expression in rat T9 glioma cells up to 24 hours, beyond which the HSP levels plummeted.

It is important to note that cells with elevated HSP levels possess an increased ability (~4–10-fold) to tolerate future hyperthermia treatments. This phenomenon, known as thermotolerance, can last from a few hours to a few weeks.[47] It needs to be emphasized that the thermotolerance phenomenon is temperature-dependent and reversible. Moderate/mild hyperthermia (ie, heating at ≤43ºC) is reported to promote thermotolerance

by inducing HSP expression in cells.[48] It has been observed that when these cells are reincubated at 37°C, HSP expression drops back to basal levels with time.[21,49] However, with an increase in temperature above a distinct threshold (usually above 43ºC), cells cannot achieve any further HSP induction and the protein-folding capacity of HSPs becomes exhausted. Overload of such non-functional HSPs causes protein misfolding and aggregation, resulting in cell death.

Keeping this fact in mind, the combined results of induction of HSPs and cell viability observed in the present study suggest that the enhanced expression of HSP70 and HSP90 after Dex-LSMO-mediated hyperthermia at 43°C is probably involved in thermotolerance, since cells could recover even after repeated cycles of hyperthermia. In contrast, the enhanced level of HSPs at 45°C and 47°C might be involved in promotion of apoptosis, since almost all the cells underwent cell death, 24 hours after repeated cycles of hyperthermia.

It is worth mentioning that HSPs are not only interesting because of their various biological functions but also because of their potential benefit in the treatment of cancer. In contrast with normal cells, tumor cells can express HSPs on their cell surface after hyperthermia. These surface-expressed HSPs (particularly HSP70 and HSP90) act as signals for the immune system and selectively sensitize tumor cells for immune attack, resulting in antitumor activity.[50–52] Based on the enhanced expression of HSP70 observed in our study, it can be safely assumed that RF-induced Dex-LSMO-mediated hyperthermia may also cause immunogenicity and result in tumor regression.
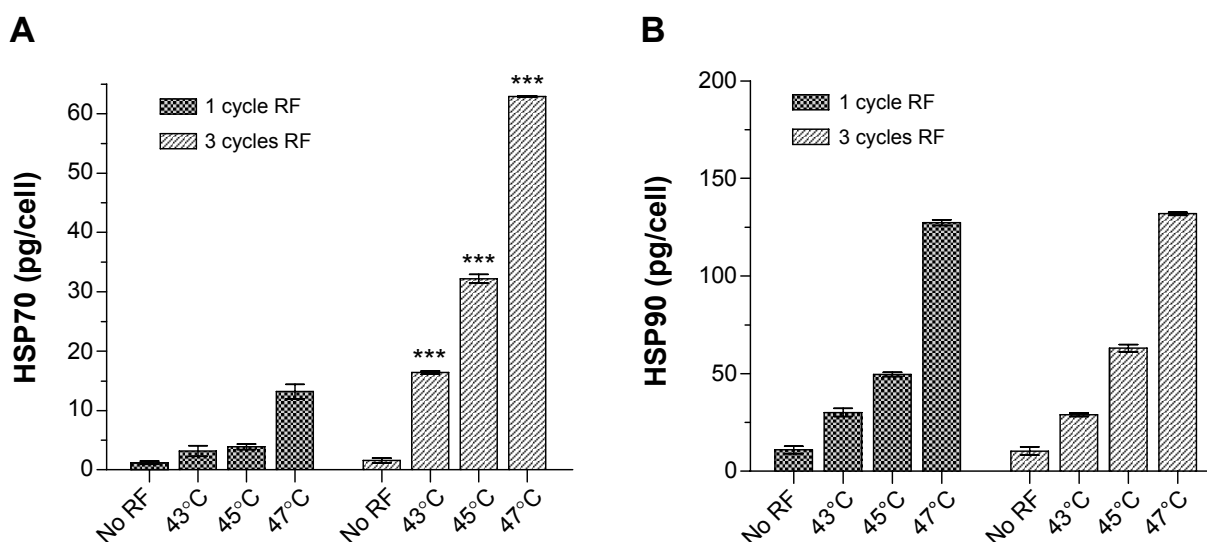
Figure 14 Induction of (**A**) HSP70 and (**B**) HSP90 after one or three cycles of RF-induced dextran-coated LSMO-mediated hyperthermia. ***P<0.001, one-way analysis of variance followed by Dunnett's test.
Abbreviations: HSP, heat shock protein; LSMO, La$_{0.7}$Sr$_{0.3}$MnO$_3$; RF, radiofrequency.

Conclusion

The present study demonstrates the excellent therapeutic efficacy of Dex-LSMO-mediated hyperthermia in melanoma cells in vitro. This treatment was able to decrease cell viability, enhance apoptosis, and induce HSP expression in a time-dependent and temperature-dependent manner. These data, along with our earlier observation of internalization of Dex-LSMO nanoparticles,[25] highlight the potential of Dex-LSMO nanoparticles as agents for inducing intracellular and localized hyperthermia to treat melanoma and other types of cancers.

Disclosure

The authors report no conflicts of interest in this work.

References

1. Jeon MJ, Ahn CH, Kim H, et al. The intratumoral administration of ferucarbotran conjugated with doxorubicin improved therapeutic effect by magnetic hyperthermia combined with pharmacotherapy in a hepatocellular carcinoma model. *J Exp Clin Cancer Res*. 2014;33(1):1–11.
2. Akbarzadeh A, Samiei M, Davaran S. Magnetic nanoparticles: preparation, physical properties, and applications in biomedicine. *Nanoscale Res Lett*. 2012;7(1):1–13.
3. Hegyi G, Szigeti GP, Szasz A. Hyperthermia versus oncothermia: cellular effects in complementary cancer therapy. *Evid Based Complement Alternat Med*. 2013;2013:672873.
4. Pollert E, Kaman O, Veverka P, et al. Core-shell $La_{1-x}S_rMnO_3$ nanoparticles as colloidal mediators for magnetic fluid hyperthermia. *Philos Trans A Math Phys Eng Sci*. 2010;368(1927):4389–4405.
5. Chatterjee DK, Diagaradjane P, Krishnan S. Nanoparticle-mediated hyperthermia in cancer therapy. *Ther Deliv*. 2011;2(8):1001–1014.
6. Moroz P, Jones SK, Gray BN. Magnetically mediated hyperthermia: current status and future directions. *Int J Hyperthermia*. 2002;18(4):267–284.
7. Habash RWY, Bansal R, Krewski D, Alhafid HT. Thermal therapy. Part 2: hyperthermia techniques. *Crit Rev Biomed Eng*. 2006;34(6):491–542.
8. Silva AC, Oliveira TR, Mamani JB, et al. Application of hyperthermia induced by superparamagnetic iron oxide nanoparticles in glioma treatment. *Int J Nanomedicine*. 2011;6(3):591–603.
9. Cheng D, Li X, Zhang G, Shi H. Morphological effect of oscillating magnetic nanoparticles in killing tumor cells. *Nanoscale Res Lett*. 2014;9(1):1–8.
10. Ito A, Shinkai M, Honda H, Kobayashi T. Medical application of functionalized magnetic nanoparticles. *J Biosci Bioeng*. 2005;100(1):1–11.
11. Mikhaylov G, Mikac U, Magaeva AA, et al. Ferri-liposomes as a novel MRI-visible drug delivery system for targeting tumors and their microenvironment. *Nat Nanotechnol*. 2011;6(9):594–602.
12. Martinez-Boubeta C, Balcells L, Cristofol R, et al. Self-assembled multifunctional Fe/MgO nanospheres for magnetic resonance imaging and hyperthermia. *Nanomedicine*. 2010;6(2):362–370.
13. Wang YM, Cao X, Liu GH, et al. Synthesis of Fe_3O_4 magnetic fluid used for magnetic resonance imaging and hyperthermia. *J Magn Magn Mater*. 2011;323(23):2953–2959.
14. Goya GF, Asin L, Ibarra RM. Cell death induced by AC magnetic fields and magnetic nanoparticles: current state and perspectives. *Int J Hyperthermia*. 2013;29(8):810–818.
15. Roti Roti JL. Cellular responses to hyperthermia (40°C–46°C): cell killing and molecular events. *Int J Hyperthermia*. 2008;24(1):3–15.
16. Harmon BV, Corder AM, Collins RJ, et al. Cell death induced in a murine mastocytoma by 42°C–47°C heating in vitro: evidence that the form of death changes from apoptosis to necrosis above a critical heat load. *Int J Radiat Biol*. 1990;58(5):845–858.
17. Cherukuri P, Glazer ES, Curley SA. Targeted hyperthermia using metal nanoparticles. *Adv Drug Deliv Rev*. 2010;62(3):339–345.
18. Todaka T, Kishino T, Enokisono N. Low Curie temperature material for induction heating self-temperature controlling system. *J Magn Magn Mater*. 2008;320(20):702–707.
19. Daengsakul S, Thomas C, Thomas I, et al. Magnetic and cytotoxicity properties of $La_{1-x}S_{rx}MnO_3$ ($0 \leq \times \leq 0.5$) nanoparticles prepared by a simple thermal hydro-decomposition. *Nanoscale Res Lett*. 2009;4(8):839–845.
20. Thorat ND, Khot VM, Salunkhe AB, Ningthoujam RS, Pawar SH. Functionalization of $La_{0.7}Sr_{0.3}Mn_{O3}$ nanoparticles with polymer: studies on enhanced hyperthermia and biocompatibility properties for biomedical applications. *Colloids Surf B Biointerfaces*. 2013;104:40–47.
21. Bhayani KR, Rajwade JM, Paknikar KM. Radio frequency induced hyperthermia mediated by dextran stabilized LSMO nanoparticles: in vitro evaluation of heat shock protein response. *Nanotechnology*. 2013;24(1):015102.
22. Kale SN, Aurora S, Bhayani KR, et al. Cerium doping and stoichiometry control for biomedical use of $La_{0.7}Sr_{0.3}Mn_{O3}$ nanoparticles: microwave absorption and cytotoxicity study. *Nanomedicine*. 2006;2(4):217–221.
23. Bhayani KR, Kale SN, Aurora S, et al. Protein and polymer immobilized $La_{0.7}Sr_{0.3}Mn_{O3}$ nanoparticles for possible biomedical applications. *Nanotechnology*. 2007;18(34):345101.
24. Balivada S, Rachakatla RS, Wang H, et al. A/C magnetic hyperthermia of melanoma mediated by iron(0)/iron oxide core/shell magnetic nanoparticles: a mouse study. *BMC Cancer*. 2010;10(119):1–9.
25. Haghniaz R, Bhayani KR, Umrani RD, Paknikar KM. Dextran stabilized lanthanum strontium manganese oxide nanoparticles for magnetic resonance imaging. *RSC Adv*. 2013;3(40):18489–18497.
26. Faraji AH, Wipf P. Nanoparticles in cellular drug delivery. *Bioorg Med Chem*. 2009;17(8):2950–2962.
27. Schweiger C, Hartmann R, Zhang F, Parak WJ, Kissel TH, Rivera-Gil P. Quantification of the internalization patterns of superparamagnetic iron oxide nanoparticles with opposite charge. *J Nanobiotechnology*. 2012;10(28):1–11.
28. Ravi V, Kullkarni SD, Samuel V, et al. Synthesis of $La_{0.7}Sr_{0.3}Mn_{O3}$ at 800°C using citrate gel method. *Ceram Int*. 2006;33(6):1129–1132.
29. Thorat ND, Shinde KP, Pawar SH, Barick KC, Bettyc CA, Ningthoujamc RS. Polyvinyl alcohol: an efficient fuel for synthesis of superparamagnetic LSMO nanoparticles for biomedical application. *Dalton Trans*. 2012;41(10):3060–3071.
30. Rajagopal R, Jani M, Kale SN, et al. $La_{0.7}Sr_{0.3}Mn_{O3}$ nanoparticles coated with fatty amine. *Appl Phys Lett*. 2006;89(2):023107.
31. Islam N, Abbas M, Sinha B, Joeng JR, Kim C. Silica encapsulation of sonochemically synthesized iron oxide nanoparticles. *Electron Mater Lett*. 2013;9(6):817–820.
32. Prasad NK, Rathinasamy K, Panda D, Bahadur D. TC-tuned biocompatible suspension of $La_{0.73}Sr_{0.27}Mn_{O3}$ for magnetic hyperthermia. *J Biomed Mater Res B*. 2008;85(2):409–416.
33. Khosroshahi ME, Ghazanfari L, Hasan-Nejad Z. Preliminary results of treating cancerous cells of lung (QU-DB) by hyperthermia using diode laser and gold coated Fe_3O_4/SiO_2 nano-shells: an in-vitro assay. *Iran J Med Phys*. 2012;9(4):253–263.
34. Nakayama J, Kageshita T, Nakashima M, Tsujisaki M, Imai K, Hori Y. Increase in shedding of intercellular adhesion molecule-1 in human malignant melanoma cell lines treated with hyperthermia in vitro. *Pigment Cell Res*. 1996;9(3):154–158.
35. Fukao H, Ikeda M, Ichikawa T, et al. Effect of hyperthermia on the viability and the fibrinolytic potential of human cancer cell lines. *Clin Chim Acta*. 2000;296(1):17–33.

36. Milani V, Frankenberger B, Heinz O, et al. Melanoma-associated antigen tyrosinase but not Melan-A/MART-1 expression and presentation dissociate during the heat shock response. *Int Immunol*. 2005;17(3):257–268.

37. Garcia MP, Cavalheiro JRT, Fernandes MH. Acute and long-term effects of hyperthermia in B16-F10 melanoma cells. *PLoS One*. 2012;7(4): e35489.

38. Ito A, Shinkai M, Honda H, Wakabayashi T, Yoshida J, Kobayashi T. Augmentation of MHC class I antigen presentation via heat shock protein expression by hyperthermia. *Cancer Immunol Immunother*. 2001;50(10): 515–522.

39. Gao F, Cai Y, Zhou J, et al. Pullulan acetate coated magnetite nanoparticles for hyperthermia: preparation, characterization and in vitro experiments. *Nano Res*. 2010;3(1):23–31.

40. Bakshi H, Sam S, Rozati R, et al. DNA fragmentation and cell cycle arrest: a hallmark of apoptosis induced by crocin from Kashmiri saffron in a human pancreatic cancer cell line. *Asian Pac J Cancer Prev*. 2010; 11(3):675–679.

41. Collins RJ, Harmon BK, Gobe GC, Kerr JFR. Internucleosomal DNA cleavage should not be the sole criterion for identifying apoptosis. *Int J Radiat Biol*. 1992;61(4):451–453.

42. Nikoletopoulou V, Markaki M, Palikaras K, Tavernarakis N. Crosstalk between apoptosis, necrosis and autophagy. *Biochim Biophys Acta*. 2013;1833(12):3448–3459.

43. Ouyang L, Shi Z, Zhao S, et al. Programmed cell death pathways in cancer: a review of apoptosis, autophagy and programmed necrosis. *Cell Prolif*. 2012;45(6):487–498.

44. Sharif-Khatibi L, Kariminia A, Khoei S, Goliaei B. Hyperthermia induces differentiation without apoptosis in permissive temperatures in human erythroleukaemia cells. *Int J Hyperthermia*. 2007;23(8):645–655.

45. Nijhuis EH, Poot AA, Feijen J, Vermes I. Hsp70- and p53-reponses after heat treatment and/or X-irradiation mediate the susceptibility of hematopoietic cells to undergo apoptosis. *Int J Radiat Biol*. 2008; 84(2):99–105.

46. Vigor KL. Antibody targeted nanoparticles for imaging and therapy of cancer. Doctoral dissertation. London, UK: University College London; 2010.

47. Christophi C, Winkworth A, Muralihdaran V, Evans P. The treatment of malignancy by hyperthermia. *Surg Oncol*. 1998;7(1):83–90.

48. Samali A, Holmberg CI, Sistonen L, Orrenius S. Thermotolerance and cell death are distinct cellular responses to stress: dependence on heat shock proteins. *FEBS Lett*. 1999;461(3):306–310.

49. Tang Y. Cancer therapy combining modalities of hyperthermia and chemotherapy: in vitro cellular response after rapid heat accumulation in the cancer cell. Doctoral dissertation. Miami, FL, USA: Florida International University; 2010.

50. Multhoff G, Botzler C, Wiesnet M, et al. Stress-inducible 72-kDa heat-shock protein (HSP72) is expressed on the surface of human tumor cells, but not on normal cells. *Int J Cancer*. 1995;61(2):272–279.

51. Sreedhar AS, Csermely P. Heat shock proteins in the regulation of apoptosis: new strategies in tumor therapy: a comprehensive review. *Pharmacol Ther*. 2004;101(3):227–257.

52. Torigoe T, Tamura Y, Sato N. Heat shock proteins and immunity: application of hyperthermia for immunomodulation. *Int J Hyperthermia*. 2009;25(8):610–616.